Colloids and Surfaces A: Physicochem. Eng. Aspects 459 (2014) 217–224

Contents lists available at ScienceDirect

Colloids and Surfaces A: Physicochemical and Engineering Aspects

journal homepage: www.elsevier.com/locate/colsurfa

Controlling air solubility to maintain "Cassie" state for sustained drag reduction

D. Dilip, Narsing K. Jha, Raghuraman N. Govardhan, M.S. Bobji *

Department of Mechanical Engineering, Indian Institute of Science, Bangalore 560012, India

HIGHLIGHTS

- Underwater sustainability of the "Cassie" state of wetting on a textured hydrophobic surface in a microchannel is investigated.
- By controlling air solubility in water through pressure, we show that trapped air pockets on the surface can be grown or shrunk.
- Size of the air pockets is found to have a direct bearing on the measured pressure drop across the channel.
- Maximum drag reduction is realized when air pockets are flush with the surface.

GRAPHICAL ABSTRACT

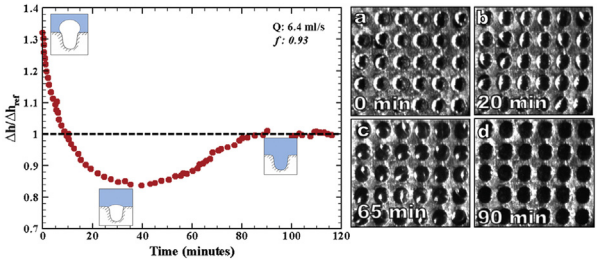

ARTICLE INFO

Article history:
Received 10 May 2014
Received in revised form 30 June 2014
Accepted 3 July 2014
Available online 14 July 2014

Keywords:
Cassie state
Textured Hydrophobic surface
Trapped air bubbles
Solubility
Sustained drag reduction

ABSTRACT

"Cassie" state of wetting can be established by trapping air pockets on the crevices of textured hydrophobic surfaces, leading to significant drag reduction. However, this drag reduction cannot be sustained due to gradual dissolution of trapped air into water. In this paper, we explore the possibility of sustaining the underwater Cassie state of wetting in a microchannel by controlling the solubility of air in water; the solubility being changed by controlling the local absolute pressure near the surface. We show that using this method, we can in fact make the water locally supersaturated with air thus encouraging the growth of trapped air pockets on the surface. In this case, the water acts as a pumping medium, delivering air to the crevices of the hydrophobic surface in the microchannel, where the presence of air pockets is most beneficial from the drag reduction perspective. In our experiments, the air trapped on a textured surface is visualized using total internal reflection based technique, at different local absolute pressures with the pressure drop (or drag) also being simultaneously measured. We find that, by controlling the pressure and hence the solubility close to the surface, we can either shrink or grow the trapped air bubbles, uniformly over a large surface area. The experiments show that, by precisely controlling the pressure and hence the solubility we can sustain the "Cassie state" over extended periods of time. This method thus provides a means of getting sustained drag reduction from a textured hydrophobic surface in channel flows.

* Corresponding author. Tel.: +91 8022933233.
E-mail addresses: dilip9375@gmail.com (D. Dilip), navinnaru88@gmail.com (N.K. Jha), raghu@mecheng.iisc.ernet.in (R.N. Govardhan), bobji@mecheng.iisc.ernet.in (M.S. Bobji).
URL: http://www.mecheng.iisc.ernet.in/ bobji/ (M.S. Bobji).

http://dx.doi.org/10.1016/j.colsurfa.2014.07.006
0927-7757/

1. Introduction

Superhydrophobic surfaces with very large contact angles can be realized by trapping air on the hydrophobic surfaces, by controlling the surface roughness or texture [1–7], to establish "Cassie state" of wetting. Design and development of such superhydrophobic surfaces has been largely inspired by nature and has been reviewed recently [8,9]. In nature, some insects use underwater hydrophobicity to maintain an air layer, plastron [10], and use it to breathe while underwater. A biomimetic plastron made from superhydrophobic material could be helpful in many underwater applications [11,12]. Usage of such surfaces can lead to drag reduction not only in internal flow situations [13–20] but also in external flow [21]. In addition to drag reduction, superhydrophobic surfaces have also been used to achieve enhanced fluid mixing in microchannels [22].The phenomena of liquid slippage [16,18,19,23] experienced in flow over hydrophobic surfaces leading to drag reduction, has been attributed to the presence of air pockets on the surface [24]. Hence for many applications it is important to maintain Cassie state on surfaces immersed completely in water [25]. However, underwater Cassie state is not sustainable due to the diffusion of trapped air into water [19,26,27]. Hence, the beneficial effects such as drag reduction diminish with time. Restoring the air in to the crevices using electrolysis has been recently studied [28,29]. In this paper, we explore the possibility of sustaining the Cassie state of wetting on a textured surface, by controlling the solubility of air in water close to the surface in a microchannel.

Diffusion of air from the trapped air pockets into the surrounding water is one of the main problems in sustaining underwater Cassie state of wetting. Smaller bubbles less than 1 μm diameter can persist indefinitely on properly angled crevices in the surface as the diffusion is countered by surface tension [30]. Alternatively, Cassie state has also been sustained by maintaining the trapped air on the surfaces in the form of small nanometer sized bubbles [31]. However for drag reduction applications, it is not only the fraction of the area covered by air that is important, but the size of the air pocket is also important, as it determines the amount of drag reduction. Larger the air pocket, larger is the reduction in drag [32]. For air pockets larger than 1 μm, diffusion effects dominate, and hence Cassie state cannot be sustained for very long. Very large bubbles may also become unstable due to decreased pressure difference across the interface and any small fluctuation in the pressures will collapse the bubble causing a Cassie to Wenzel wetting transition. This wetting transition and thus the sustainability of the Cassie state depends not only on the hydrostatic pressure but also on the kind of texture [26] that determines the effective pinning of the two phase line. Bobji et al.[26] showed that surfaces with holes exhibit better characteristics in retaining the Cassie state of wetting.

Rate of diffusion of air across the water–air interface depends on the concentration gradient of air across the interface. For example, superhydrophobic lotus leaf turns to completely wetting Wenzel state when immersed in water for a few minutes or when exposed to high hydrostatic pressures [33,34]. More generally, switching between Cassie and Wenzel state can be achieved by varying the pressure [35]. In addition, under flow conditions, removal of entrapped air is enhanced by stronger convection at larger flow rates [36]. The overall result is that the air pockets trapped on the surface will gradually shrink and eventually disappear. The time scale for this depends on both the concentration gradient as well as the velocity of the flow. In order to sustain the Cassie state in the presence of flow, it is thus necessary to continuously supply air to the trapped air pockets. Directly supplying air has been tried out in microchannel flows through a self regulating mechanism [37,38] involving complex arrangements with active feedback control. In this work, we explore the possibility of supplying air to the cavities on the surface of a microchannel by controlling the solubility of air in water close to the surface. This is achieved in the present work by adjusting the absolute pressure of water close to the surface without the need for any complex feedback controls.

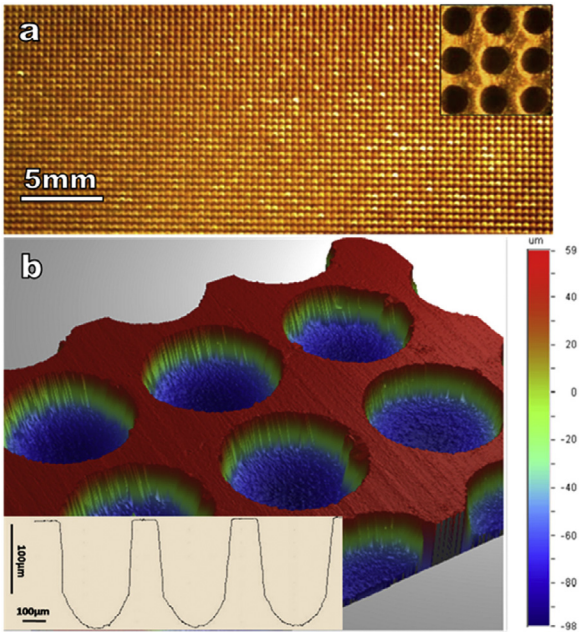

Fig. 1. (a) Textured brass surface containing a regular array of blind holes. The surface dimensions are 100 mm × 30 mm. The inset shows a zoomed-in view (1 mm × 1 mm) of the blind holes in which air can be trapped. (b) Surface profile of the textured hydrophobic surface used for the experiment obtained using an optical profilometer. Inset shows the contour of the surface. Hole diameter is 300 μm, pitch 365 μm and depth 160 μm.

As the solubility decreases with pressure, a lower absolute pressure close to the surface can lead to water becoming locally supersaturated with air. This can lead to the concentration gradient being reversed and hence air can actually start diffusing into the air pockets causing them to grow as a bubble. We demonstrate this effect using a hydrophobic surface textured with a regular array of holes in a microchannel configuration. We show that, in internal flow conditions, by carefully controlling the pressure, we can get the trapped air pockets within the holes to either diminish or grow, and also alter the rate of shrinkage or growth of these air pockets. This enables us to sustain a regular array of air pockets on the surface over a very large area leading to sustained drag reduction over extended time periods.

2. Experimental methods

A textured surface was generated on a brass sheet of dimensions 100 mm × 30 mm × 0.8 mm by photo etching process. The texture consists of blind holes of diameter 0.3 mm arranged in a 0.36 mm × 0.36 mm square array (Fig. 1a). After laminating with a photo resist, the desired pattern was transferred by exposing the resist to ultraviolet light through a mask. Etching was carried out with heated solution of cupric chloride and the depth was controlled by controlling the duration of etching. A texture consisting of a regular array of blind holes was chosen due to the superior ability to trap air bubbles [26]. Fig. 1a shows optical image of a part of the textured hydrophobic surface with the inset showing a magnified view of the blind holes. It can be seen that a regular array has been produced over a very large surface area. The depth of the holes was measured using a 3D non-contact profilometer (Fig. 1b). The depth of the blind holes was found to be 160±10 μm, and the diameter and the pitch were found to be uniform across the surface with dimensions of 300±10 μm and 365±10 μm, respectively.

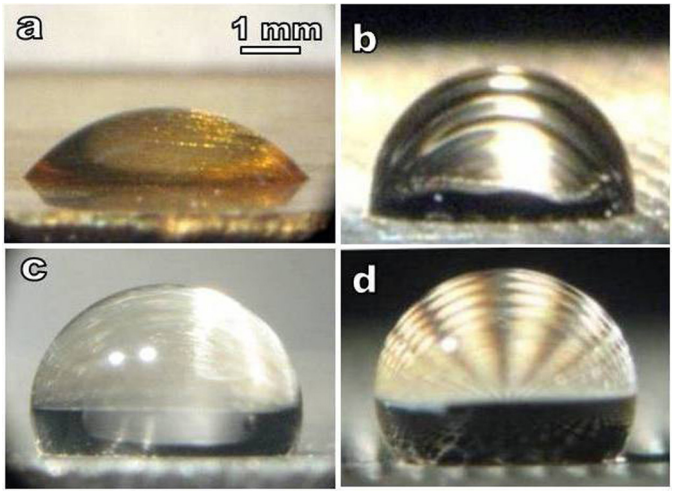

Fig. 2. Contact angle measured on (a) smooth brass surface (b) textured brass surface with holes (c) smooth hydrophobic surface and (d) textured hydrophobic surface.

The brass surface is rendered hydrophobic by a self assembled monolayer (SAM). For this, the surface was immersed in a 50 mM solution of 1-dodecanethiol in ethanol, for 2 h [39,40]. The surface was then dried in an oven at 60 °C. Contact angle (θ_m) measurements were carried out with a 10 μL deionized water droplet and are shown in Fig. 2. A flat smooth surface of brass has a contact angle of about 43° which increases to 106° after SAM coating. Textured surface without SAM gave a contact angle of 84°. It should be noted that the roughness factor, r is about 2.2 for this surface. After depositing SAM on the textured surface the contact angle increased to 124°. If air is trapped inside all the holes, then the air fraction ϕ would be about 0.55. The contact angles measured and those estimated from the Wenzel (θ_w) and Cassie–Baxter (θ_c) equations [41,42] are given in Table 1.

A microchannel arrangement in which the textured hydrophobic surface serves as one of its walls is used to study the behavior of the trapped air pockets. A hydrophilic flat transparent glass surface forms the other wall of the channel so that the trapped air pockets can be easily visualized. The channel walls are separated by a stainless steel spacer so as to maintain a channel width of 1 mm. Water is induced to flow through the channel by gravity. The schematic of the arrangement is shown in Fig. 3a. The absolute pressure inside the channel is controlled by changing the relative height of the water tank with respect to the channel. The water level in the tank is maintained constant by an overflow arrangement. When a pressure lesser than the atmospheric pressure is required inside the channel, the water level in the source tank is maintained below the channel level so that water flows through the channel by siphon effect.

The trapped air bubbles are visualized by using total internal reflection (TIR) of light [19,26]. For this the channel is placed inside a glass tank filled with stationary water (Fig. 3b) and a parallel beam of light is made to incident on the surface at an angle greater than the critical angle

$$\psi = \sin^{-1}\left(\frac{1}{n}\right) \quad (1)$$

required for total internal reflection, where n is the refractive index of water. The beam would undergo total internal reflection at the water–air interface and the trapped air bubbles would appear distinctly bright. By using a camera attached to an optical microscope, images of air bubbles are recorded at regular intervals of time. Prior to the experiments, air is allowed to be dissolved in the water by allowing the water to be exposed to atmospheric air in a large tank overnight. Just before the experiment, the channel is first dried and flushed with dry nitrogen for about 30 min. The channel is then filled with water from the tank very slowly such that air bubbles are trapped inside the holes uniformly throughout the surface. This process is repeated before each trial and flow is induced through the channel only after optically checking that there is uniform coverage of air bubbles throughout the surface.

3. Results and discussion

When the absolute water pressure in the channel is maintained above the atmospheric pressure by adjusting the height of the tank appropriately (Fig. 3a), the water flowing in the channel past the air pockets will be undersaturated. In such conditions, the air pockets gradually decrease in size. Fig. 4 shows a time sequence of images at an absolute pressure of 6.8 kPa above atmospheric pressure. In this case, the flow rate is 6.4 mL/s with the flow being from left to right in all the images shown (Supplementary Video 1). In each of the cases, the inset schematically shows the bubble size. At the start of the experiment, the air pockets were allowed to grow slightly by exposing the surface to supersaturated flowing water, resulting in air pockets that have grown into a bubble that is projecting into the flow as seen in Fig. 4a. After about 20 min, these bubbles have shrunk in size with the contact line firmly pinned on the edges of the hole, as shown in the inset (Fig. 4b). Eventually the pinning gives way and the bubbles move into the holes with de-pinning starting preferentially at the leading edge on the left (Fig. 4c). This may be related to the drag force on the bubble, which would push the bubble from left to right. By about 90 min, no air pockets could be detected (Fig. 4d). This could mean either that the air pockets are too small to be detected or that they have completely disappeared.

Supplementary Video 1 related to this article can be found, in the online version, at http://dx.doi.org/10.1016/j.colsurfa.2014.07.006.

Fig. 5 shows the time sequence when the absolute pressure in the channel is maintained below atmospheric pressure (by 4.4 kPa) by adjusting the height of the tank appropriately (Supplementary Video 2). In this case, the water is supersaturated with air resulting in the observed growth of the trapped air pockets. The flow rate through the channel is maintained as before at 6.4 mL/s by appropriate adjustments of sink or receiving tank height. Fig. 5a shows the air pockets at the start of the experiment. At about 5 min after the commencement of flow through the channel, the bubbles have grown bigger (Fig. 5b). After 13 min, the air bubbles have grown further and appear to be protruding out of the holes (Fig. 5c). The

Table 1
Measured and estimated contact angles on the smooth and textured surfaces used.

Surface	Measured contact angle θ_m(°)	Estimated Wenzel contact angle θ_w(°)	Estimated Cassie contact angle θ_c(°)
Smooth brass	43	–	–
Smooth brass with SAM	106	–	–
Textured	84	Unstable [a]	101
Textured with SAM	124	127	131

[a] Indicates $\cos\theta_w > 1$.

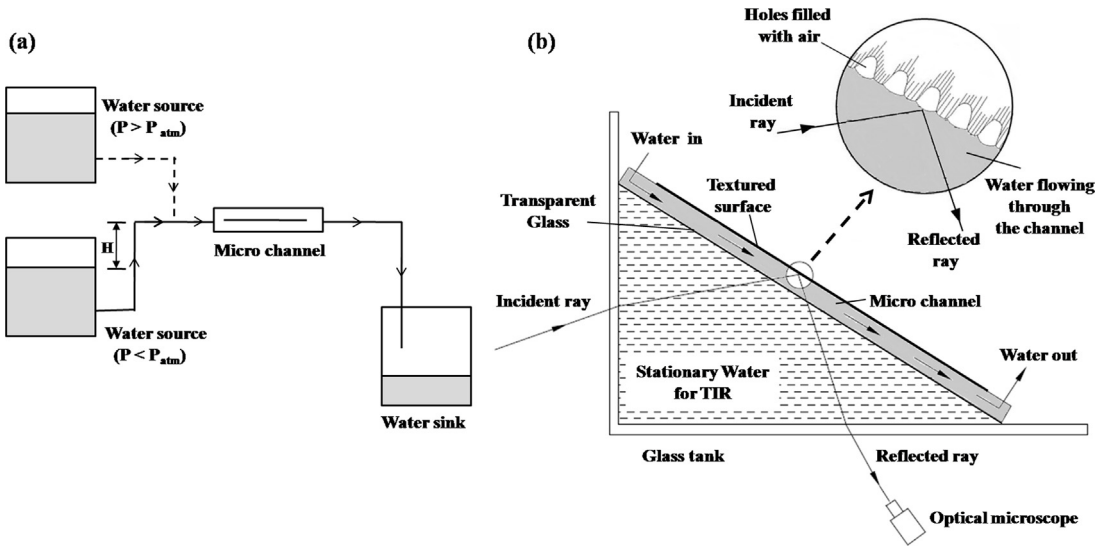

Fig. 3. (a) Schematic of experimental setup. A pressure greater than atmospheric pressure is maintained inside the channel by gravity flow from a water tank. Sub-atmospheric pressure is maintained inside the channel whenever required by means of siphon effect. (b) Schematic of the setup used for visualization. The sealed channel flow system is placed inside a glass tank filled with water and a light beam is incident on the textured surface at an angle greater than the critical angle required so that the light undergoes total internal reflection at the water–air interface.

progressive growth of air bubbles continue with time and by 17 min (Fig. 5d), the bubble protrusion into the flowing water becomes more pronounced. If the flow is continued further, the bubbles grow even bigger and start merging with neighboring bubbles.

Supplementary Video 2 related to this article can be found, in the online version, at http://dx.doi.org/10.1016/j.colsurfa.2014.07.006.

The rate of change of the size of the air pockets depends on the absolute pressure in the channel which in turn controls the saturation level, and the flow rate. Fig. 6 shows how the diameter of the bubbles varies with time for various pressures at a flow rate of 6.4 mL/s. The bubble diameter, D, at any instant is normalized with respect to the initial size of the bubble D_i. The bubble diameters are measured from time lapse images recorded at an interval of 30 seconds. At pressures lesser than atmospheric, the growth of air bubbles is evident from the increase in D/D_i. As the pressure is decreased, it can be seen that the rate of growth of air bubbles increases. On the contrary, at pressures above the atmospheric pressure, the size of the bubbles decreases with time. As the pressure is increased, the rate of decrease in the diameter also increases. At a pressure of +3.9 kPa, the bubbles decrease to about 80% of their original size in about 80 min. It may be noted that measurement of bubble diameters below 70% of the original bubble size is difficult as the triple interface line moves into the holes and is not visible.

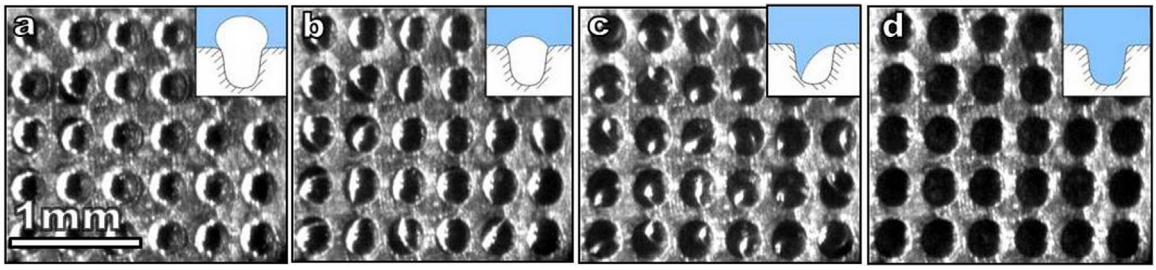

Fig. 4. Time sequence of images showing the shrinkage of air bubbles at a pressure of 6.8 kPa above the atmospheric pressure at a flow rate of 6.4 mL/s through the channel. The times during shrinkage are (a) $t = 0$ min, (b) $t = 20$ min, (c) $t = 65$ min and (d) $t = 90$ min. The schematic shown as inset in each image indicates the size of the bubble. The flow direction is from left to right.

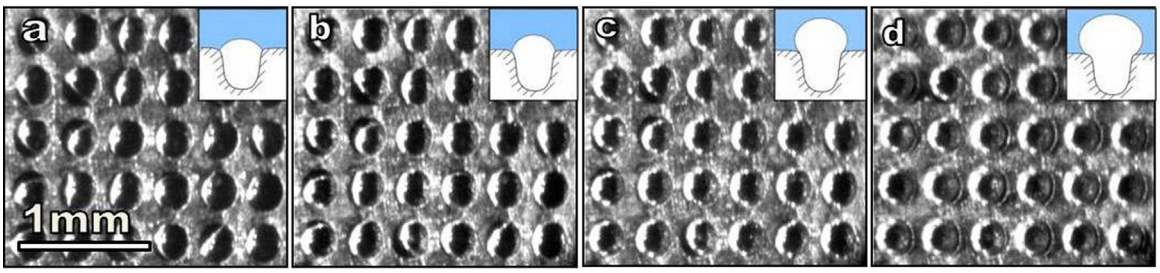

Fig. 5. Time sequence of images during the growth of air bubbles at a pressure of 4.4 kPa below the atmospheric pressure at a flow rate of 6.4 mL/s through the channel. The times after flow is started are (a) $t = 0$ min, (b) $t = 5$ min, (c) $t = 13$ min and (d) $t = 17$ min. The schematic shown as inset in each image indicates the size of the bubble. The flow direction is from left to right.

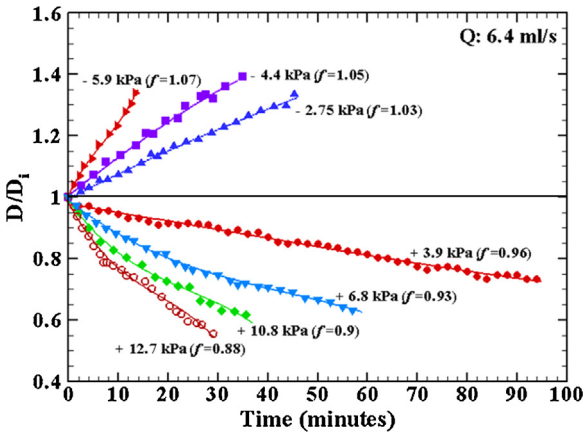

Fig. 6. Variation in bubble size with time for varying pressures at a flow rate of 6.4 mL/s through the channel. For pressures lower than atmospheric (negative pressure) the air bubbles grow with time, whereas for pressures greater than the atmospheric pressure (positive pressure), the bubbles shrink with time. At higher negative pressures the rate of increase in bubble size is higher. At higher positive pressures, the rate of shrinkage of air bubbles is higher.

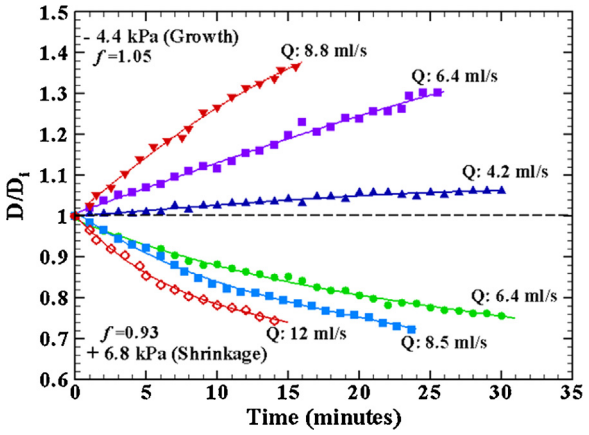

Fig. 7. Variation in bubble size with time at various flow rates at a pressure of −4.4 kPa below atmospheric pressure (f = 0.93) and at a pressure of +6.8 kPa above the atmospheric pressure (f = 1.05). The various flow rates through the channel are 4.2, 6.4 and 8.8 mL/s when the pressure is −4.4 kPa. For a pressure of +6.8 kPa the flow rates maintained are 6.4, 8.5 and 12 mL/s.

The rate of dissolution or growth of the air pockets will depend on the concentration gradient of air across the air–water interface. According to Henry's law, the concentration of the gas dissolved in liquid at saturation (C_s) is proportional to the partial pressure (p_g) of the gas at which the dissolution occurred. The concentration of air in water at saturation can be obtained as the sum of individual components of air as

$$C_i = \frac{p_O}{H_O} + \frac{p_N}{H_N} = \frac{P}{H_{air}} \tag{2}$$

where H_O and H_N are the Henry's constant for oxygen and nitrogen in water respectively and p_O and p_N are the partial pressures of oxygen and nitrogen, respectively and P is the atmospheric pressure. H_{air} can be obtained from the molar fractions of oxygen and nitrogen as,

$$H_{air} = \frac{1}{(n_O/n_{air})(1/H_O) + (n_N/n_{air})(1/H_N)} \tag{3}$$

At room temperature, the saturation concentration of air in water is about 0.0227 g/L. It should be noted that experimentally achieved values are likely to be lower than this. When water flows in the channel, the pressure inside the channel is changed by, ΔP, compared to the atmospheric pressure, P, at which the saturation took place. The saturation concentration of air in the channel at the new pressure ($P + \Delta P$) is

$$C_s = \frac{P + \Delta P}{H_{air}} \tag{4}$$

The degree of saturation (f) is then given by

$$f = \frac{C_i}{C_s} = \frac{P}{P + \Delta P} = \frac{1}{1 + (\Delta P/P)} \tag{5}$$

where $\Delta P = \rho g H$, is controlled by varying the height difference H between the water tank and the water level in the channel. By manipulating the pressure in the channel, we vary the degree of saturation by which we can effectively control the dissolution or growth of the air pockets on the textured surface.

The rate of growth or dissolution of the bubble depends on the degree of saturation f. If the flowing water is saturated, the degree of saturation $f = 1$, and hence there would not be any change in the radius of the bubble with time. At pressures higher than the atmospheric pressure, the flowing water becomes undersaturated ($f < 1$) and the adverse concentration gradient causes the diffusion of air from the bubble into the flowing water. Therefore the air bubbles gradually shrink in size. At pressures lesser than atmospheric pressure, the water becomes supersaturated ($f > 1$) and hence the concentration gradient is reversed. Hence, the dissolved air in water diffuses into the air pockets. In such cases, the water flow acts like an air pump carrying atmospheric air to the superhydrophobic surface in the channel.

The diffusion equation was solved by Epstein and Plesset [43] for a spherical bubble suspended in an infinite medium to give the change in bubble diameter with time for undersaturated and supersaturated conditions of water. In case of air bubbles that are attached to a surface, the rate of diffusion will be lower as pointed out by Liebermann [30]. For the current experimental conditions, the air bubbles are trapped inside the holes, pinned at the edges and are in proximity to each other and this affects the rate of air diffusion across the interface. In addition, the convective effects caused by the flowing water also play an important role in the rate of removal/addition of air in to the air pockets. Larger flow rates cause quicker growth or dissolution of the bubbles at supersaturated and undersaturated conditions, respectively.

The rate of change in size of the air bubbles at different flow velocities at both supersaturated and undersaturated conditions is shown in Fig. 7. It can be seen from the figure that increasing the velocity increases the rate of air transfer from or to the bubbles, which is consistent with the fact that water from far is more rapidly reaching the water–air interface, resulting in an increased effective diffusivity. At a pressure of 6.8 kPa above atmospheric pressure, the flowing water is undersaturated and the rate at which the air gets diffused out of the air pockets is higher at higher flow velocities, resulting in faster shrinkage of the bubbles. The trend is reversed for the supersaturated condition at a pressure of 4.4 kPa below atmospheric pressure. In this case, the flow aids in bringing more air into the bubbles resulting in higher bubble growth rates at increased flow rates.

Epstein–Plesset equation [43] for growth/shrinkage of a spherical bubble at supersaturated/undersaturated solution can be written in the form:

$$\left(\frac{D}{D_i}\right)^2 = 1 - mt \tag{6}$$

where m is a parameter which depends on the degree of saturation f, and the saturation concentration C_s. At small times, the data presented in Figs. 6 and 7 fit the equation well, and the parameter m can be obtained by least-squares method. The variation of the

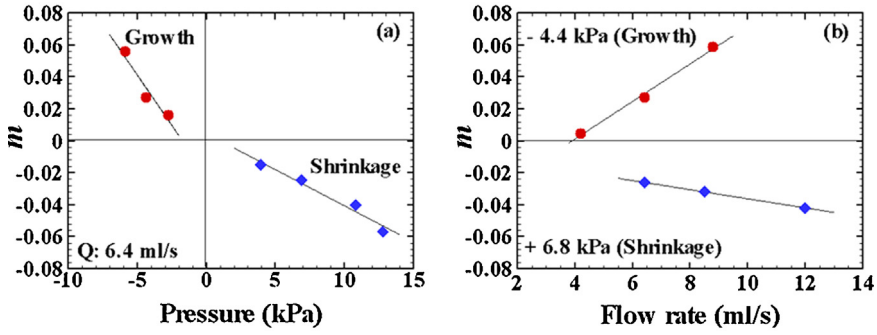

Fig. 8. Variation of parameter 'm' in Eq. (6) with (a) pressure and (b) flow rate. The pressures shown are with respect to atmospheric pressure.

parameter m with pressure and flow rate is shown in Fig. 8(a) and (b), respectively. It is apparent from Fig. 8a that the parameter m is positive and increases as the pressure becomes more negative. This trend is reversed for pressures above atmospheric pressure. The effect of flow rate on the rate of bubble growth or shrinkage is shown in Fig. 8b. At larger flow rates, the parameter m is seen to increase for positive pressures and decrease for negative pressures. The variations of the parameter m with both pressure and flow rate are reflective of the changes in the rate of growth/shrinkage of the air pocket as indicated by Eq. (6).

The air pockets offer very liitle resistance to the flow compared to the solid walls. Hence the overall pressure drop, measured across the channel length of 100 mm, is expected to be lower. The texture has been designed to give a 55% shear-free region spread over about 23,000 pockets. Fig. 9 shows the actual experimentally measured pressure drop (Δh). In this case, the air pockets were initially allowed to grow in supersaturated solution due to reduced absolute pressure. As the air pockets grow from the initially trapped condition, the pressure drop was found to increase gradually with time. At about 15 min corresponding to the dashed line in the plot, the absolute pressure was increased rendering the water undersaturated. This immediately leads to shrinking of the trapped air pockets, which in turn leads to the observed decrease in pressure drop with time. The pressure drop is observed to reach a minimum value and then start to increase slowly. Ultimately, the pressure drop reaches a constant value when all the air bubbles have disappeared. This value, Δh_{ref}, shown by a dotted line, is taken as the reference value and has been used to normalize all the measured pressure drop values (Δh) in Fig. 9.

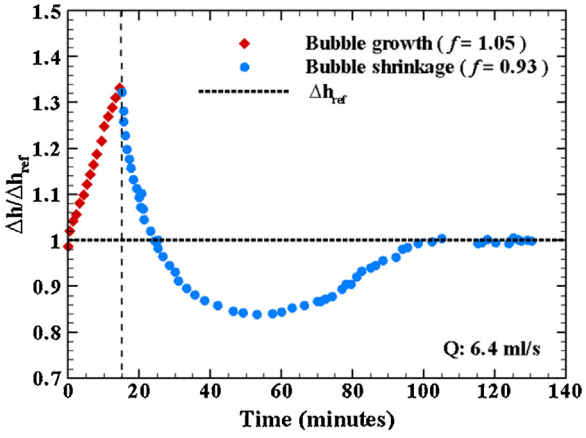

Fig. 9. Effect of growth and shrinkage of air bubbles on pressure drop at a flow rate of 6.4 mL/s through the channel. As air bubbles grow, the pressure drop also increases. When the bubbles shrink, the pressure drop decreases, reaches a minimum value and then increase till it reaches the reference pressure drop.

As the air pockets grow into bubbles, they project into the flow and start obstructing the flow. The resistance offered by the projecting bubbles will offset the drop in resistance caused due to the shear-free surface offered by air pockets. Thus the effective drag reduction obtained will depend on the geometry of the air–water interface. Fig. 10 shows the pressure drop data from Fig. 9 (time >15 min) plotted against the bubble diameter D, normalized with the diameter of the hole D_h. The bubble diameter can be related to the amount of projection by simple geometry. For higher bubble size and hence higher obstruction, the pressure drop across the channel is larger. As the bubble size decreases, the pressure drop also decreases and reaches a minimum. However, further decrease in the bubble size causes the pressure drop to increase slowly. The pressure drop reaches a constant value when all the air bubbles have disappeared. The minimum pressure drop occurs when D/D_h is close to 1, i.e., when the bubbles are almost flush with the holes. The inset to the figure shows schematics of the bubble at corresponding time instants.

The amount of drag reduction achievable is found to be influenced by the shape of the air–water interface. When the air pockets are flush with the surface, maximum drag reduction is obtained. The drag reduction obtained is reduced for both higher and lower diameters of the bubbles. For bubble diameters greater than 1.2 times the hole diameter, it has been found that the pressure drop and hence the drag is actually higher than the reference Wenzel case. This observation is consistent with the results of theoretical and numerical studies of Davis and Lauga [44], Steinberger et al.

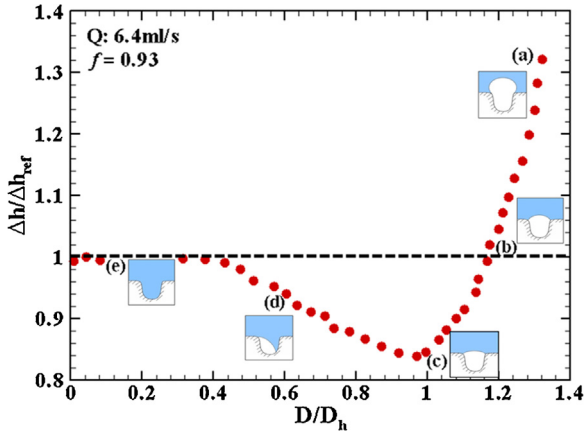

Fig. 10. Effect of bubble size on pressure drop during shrinkage of air bubbles at a degree of saturation f = 0.93 and a flow rate of 6.4 mL/s through the channel. (a) At large bubble size the pressure drop is high. (b) As the bubble shrinks pressure drop also reduces. (c) When the bubble is almost flush with the holes, the pressure drop is minimum. (d) As air bubbles decay further the pressure drop increases as water starts filling the holes. (e) Hole is completely filled with water and pressure drop has increased and become equal to the reference pressure drop.

[45] and Hyvaluoma and Harting [46]. In this work, using simultaneous bubble visualization and pressure drop measurements, we have experimentally studied the effect of bubble shape on drag reduction. Our ability to vary the local saturation of the air in water enabled the precise control of the bubble size and hence their protrusion uniformly over a large surface area. Controlling the bubble shape uniformly over large area is crucial to experimentally establish the link between bubble shape and drag, as even one large bubble would significantly affect the pressure drop measurement and hence mask the drag reduction.

In the current experiments, a maximum pressure drop reduction of 15% was obtained. Slip length λ, a measure of drag reduction, is defined as the ratio of the velocity of the water layer in contact with the surface to the velocity gradient at the surface, and may be calculated from the measured pressure drop [16]. Larger the reduction in pressure drop, higher is the slip length. For a pressure drop of 15%, slip length (λ) works out to be about 50 μm. This slip length when normalized with the hole radius R of 150 μm gives a λ/R value of 0.33. From numerical simulations, Hyvaluoma and Harting [46] obtained a value of λ/R of about 0.26 which is reasonably close to the present experimentally obtained value. It should be noted however that there are a number of additional factors that can influence slip length, as discussed by Lauga and Stone [32], such as the ratio of shear-free region (hole-size) to channel width.

Sustainability can be quantified by defining it as the time over which the drag reduction is above a certain desired value. For example, for a degree of saturation of $f = 0.93$, from the data in Fig. 9, the drag reduction is greater than 10% (i.e $\Delta h/\Delta h_{ref} < 0.9$) over a time period of 65 min. This time period is dependent on the size of the air bubbles on the surfaces which keeps on decreasing with time. For high sustainability, the rate at which the size decreases should be small tending towards zero. From Fig. 6, it is clear that as the degree of saturation is gradually increased towards one, the rate of change in bubble size decreases. Our measurements show that for a degree of saturation of 0.96, the measured sustainability is about 170 min. The only difference between the two cases is a reduction in pressure within the channel, which in effect reduces the saturation concentration. Thus by controlling the solubility through the pressure, it is possible to maintain the underwater Cassie state of wetting such that significant drag reduction can be realized and sustained over long periods of time.

4. Conclusion

Underwater Cassie state cannot be sustained for long periods of time on a textured hydrophobic surface as the air trapped in the crevices of the surface can diffuse into water. For many applications, it is desirable that large air pockets be maintained indefinitely. In this paper, we have demonstrated a simple method for sustaining the underwater Cassie state in a microchannel by controlling the solubility of air in water. For this, we use a textured surface comprising of a regular array of holes with a self assembled hydrophobic layer as one of the walls of the channel. Solubility of air in the water close to the surface is varied by varying the absolute pressure inside the channel. We use a total internal reflection based visualization method to observe the air trapped on the patterned surface, and determine the variation of the trapped air bubbles on the surface with time.

We find that when the pressure in the channel was higher than the atmospheric pressure, the air pockets gradually shrunk in size with time and eventually disappeared. On the other hand, when the pressure in the channel was decreased below atmospheric pressure, we find that the size of the air pockets gradually increased with time. In this case, the water, which was initially allowed to saturate at atmospheric pressure, when subjected to a lower pressure in the channel, becomes supersaturated. Thus the water flow acts as an air pump delivering air from the atmosphere to the desired location on the textured surface. We also find that changing the flow rate, significantly changes the rate of growth/shrinkage of the air pockets.

To quantify the drag reduction, we have measured the pressure drop across the microchannel while simultaneously visualizing the shape of the air bubbles trapped on the surface. We find that the least pressure drop across the channel occurs when the trapped air pockets are flush with the surface. On the other hand, when the air pockets protrude out of the surface or shrink in to the holes on the surface, we find an increased pressure drop. We have shown that, by controlling the pressure within the channel, we can control the shape of the air pockets and sustain them for extended periods of time. Thus, the present work shows that by carefully controlling the degree of saturation through pressure, the underwater "Cassie" state of wetting and hence the drag reduction can be sustained in a microchannel.

Appendix A. Supplementary Data

Supplementary data associated with this article can be found, in the online version, at http://dx.doi.org/10.1016/j.colsurfa.2014.07.006.

References

[1] S. Shibuichi, T. Onda, N. Satoh, K. Tsujii, Super water-repellent surfaces resulting from fractal structure, J. Phys. Chem. 100 (50) (1996) 19512–19517.
[2] J. Bico, C. Marzolin, D. Quéré, Pearl drops, Europhys. Lett. 47 (2) (1999) 220–226.
[3] S. Herminghaus, Roughness-induced non-wetting, Europhys. Lett. 52 (2) (2000) 165–170.
[4] Z. Yoshimitsu, A. Nakajima, T. Watanabe, K. Hashimoto, Effects of surface structure on the hydrophobicity and sliding behavior of water droplets, Langmuir 18 (15) (2002) 5818–5822.
[5] M. Callies, D. Quéré, On water repellency, Soft Matter 1 (1) (2005) 55–61.
[6] C. Dorrer, J. Rühe, Some thoughts on superhydrophobic wetting, Soft Matter 5 (1) (2009) 51–61.
[7] A. Cassie, S. Baxter, Wettability of porous surfaces, Trans. Faraday Soc. 40 (1944) 546–551.
[8] E. Celia, T. Darmanin, E. Taffin de Givenchy, S. Amigoni, F. Guittard, Recent advances in designing superhydrophobic surfaces, J. Colloid Interface Sci. 402 (2013) 1–18.
[9] N. Valipour M, F.C. Birjandi, J. Sargolzaei, Super-non-wettable surfaces: a review, Colloids Surf. A: Physicochem. Eng. Asp. 448 (2014) 93–106.
[10] M.R. Flynn, J.W. Bush, Underwater breathing: the mechanics of plastron respiration, J. Fluid Mech. 608 (2008) 275–296.
[11] N.J. Shirtcliffe, G. McHale, M.I. Newton, C.C. Perry, F.B. Pyatt, Plastron properties of a superhydrophobic surface, Appl. Phys. Lett. 89 (10) (2006) 104106.
[12] M.A. Samaha, H.V. Tafreshi, M. Gad-el Hak, Superhydrophobic surfaces: from the lotus leaf to the submarine, Comptes Rendus Mecanique 340 (1) (2012) 18–34.
[13] C.H. Choi, U. Ulmanella, J. Kim, C.-M. Ho, C.-J. Kim, Effective slip and friction reduction in nanograted superhydrophobic microchannels, Phys. Fluids 18 (8) (2006) 087105.
[14] R.S. Voronov, D.V. Papavassiliou, L.L. Lee, Review of fluid slip over superhydrophobic surfaces and its dependence on the contact angle, Ind. Eng. Chem. Res. 47 (8) (2008) 2455–2477.
[15] C.-H. Choi, K.J.A. Westin, K.S. Breuer, Apparent slip flows in hydrophilic and hydrophobic microchannels, Phys. Fluids 15 (10) (2003) 2897–2902.
[16] J. Ou, B. Perot, J.P. Rothstein, Laminar drag reduction in microchannels using ultrahydrophobic surfaces, Phys. Fluids 16 (12) (2004) 4635–4643.
[17] R. Truesdell, A. Mammoli, P. Vorobieff, F. van Swol, C.J. Brinker, Drag reduction on a patterned superhydrophobic surface, Phys. Rev. Lett. 97 (4) (2006) 044504.
[18] C. Lee, C.-H. Choi, et al., Structured surfaces for a giant liquid slip, Phys. Rev. Lett. 101 (6) (2008) 064501.
[19] R. Govardhan, G. Srinivas, A. Asthana, M. Bobji, Time dependence of effective slip on textured hydrophobic surfaces, Phys. Fluids 21 (5) (2009) 052001.
[20] G.D. Bixler, B. Bhushan, Shark skin inspired low-drag microstructured surfaces in closed channel flow, J. Colloid Interface Sci. 393 (2013) 384–396.
[21] S. Gogte, P. Vorobieff, R. Truesdell, A. Mammoli, F. van Swol, P. Shah, C.J. Brinker, Effective slip on textured superhydrophobic surfaces, Phys. Fluids 17 (5) (2005) 051701.
[22] J. Ou, G.R. Moss, J.P. Rothstein, Enhanced mixing in laminar flows using ultrahydrophobic surfaces, Phys. Rev. E 76 (1) (2007) 016304.
[23] M.A. Samaha, H. Vahedi Tafreshi, M. Gad-el Hak, Novel method to characterize superhydrophobic coatings, J. Colloid Interface Sci. 395 (2013) 315–321.

[24] X. Sheng, J. Zhang, Air layer on superhydrophobic surface underwater, Colloids Surf. A: Physicochem. Eng. Asp. 377 (1) (2011) 374–378.
[25] A. Marmur, Underwater superhydrophobicity: theoretical feasibility, Langmuir 22 (4) (2006) 1400–1402.
[26] M.S. Bobji, S.V. Kumar, A. Asthana, R.N. Govardhan, Underwater sustainability of the cassie state of wetting, Langmuir 25 (20) (2009) 12120–12126.
[27] M.A. Samaha, H.V. Tafreshi, M. Gad-el Hak, Sustainability of superhydrophobicity under pressure, Phys. Fluids 24 (11) (2012) 112103.
[28] K.A. Stephani, D.B. Goldstein, An examination of trapped bubbles for viscous drag reduction on submerged surfaces, J. Fluids Eng. 132 (4) (2010) 041303.
[29] C. Lee, C.J. Kim, Underwater restoration and retention of gases on superhydrophobic surfaces for drag reduction, Phys. Rev. Lett. 106 (1) (2011) 014502.
[30] L. Liebermann, Air bubbles in water, J. Appl. Phys. 28 (2) (2004) 205–211.
[31] A. Maali, B. Bhushan, Nanobubbles and their role in slip and drag, J. Phys. Condens. Matter 25 (18) (2013) 184003.
[32] E. Lauga, H.A. Stone, Effective slip in pressure-driven stokes flow, J. Fluid Mech. 489 (2003) 55–77.
[33] Y.-T. Cheng, D.E. Rodak, Is the lotus leaf superhydrophobic? Appl. Phys. Lett. 86 (14) (2005) 144101.
[34] J. Zhang, X. Sheng, L. Jiang, The dewetting properties of lotus leaves, Langmuir 25 (3) (2008) 1371–1376.
[35] T. Verho, J.T. Korhonen, L. Sainiemi, V. Jokinen, C. Bower, K. Franze, S. Franssila, P. Andrew, O. Ikkala, R.H. Ras, Reversible switching between superhydrophobic states on a hierarchically structured surface, Proc. Natl. Acad. Sci. 109 (26) (2012) 10210–10213.
[36] M.A. Samaha, H.V. Tafreshi, M. Gad-el Hak, Influence of flow on longevity of superhydrophobic coatings, Langmuir 28 (25) (2012) 9759–9766.
[37] C.F. Carlborg, W. van der Wijngaart, Sustained superhydrophobic friction reduction at high liquid pressures and large flows, Langmuir 27 (1) (2010) 487–493.
[38] E. Karatay, A.S. Haase, C.W. Visser, C. Sun, D. Lohse, P.A. Tsai, R.G. Lammertink, Control of slippage with tunable bubble mattresses, Proc. Natl. Acad. Sci. 110 (21) (2013) 8422–8426.
[39] M.S. Bobji, G. Balan, R.N. Govardhan, et al., Time dependent superhydrophobicity of drag reducing surfaces, in: 3rd Micro and Nano Flows Conference, Thessaloniki, Greece, 22–24 August 2011, 2011.
[40] Q. Pan, M. Wang, H. Wang, Separating small amount of water and hydrophobic solvents by novel superhydrophobic copper meshes, Appl. Surf. Sci. 254 (18) (2008) 6002–6006.
[41] R.N. Wenzel, Resistance of solid surfaces to wetting by water, Ind. Eng. Chem. 28 (8) (1936) 988–994.
[42] D. Quéré, Wetting and roughness, Annu. Rev. Mater. Res. 38 (2008) 71–99.
[43] P.S. Epstein, M.S. Plesset, On the stability of gas bubbles in liquid–gas solutions, J. Chem. Phys. 18 (1950) 1505–1509.
[44] A.M.J. Davis, E. Lauga, Geometric transition in friction for flow over a bubble mattress, Phys. Fluids 21 (1) (2009) 011701.
[45] A. Steinberger, C. Cottin-Bizonne, P. Kleimann, E. Charlaix, High friction on a bubble mattress, Nat. Mater. 6 (9) (2007) 665–668.
[46] J. Hyväluoma, J. Harting, Slip flow over structured surfaces with entrapped microbubbles, Phys. Rev. Lett. 100 (24) (2008) 246001.